Proceedings of 15th International Marine Design Conference (IMDC-2024)
June 2-6, 2024
Amsterdam, the Netherlands

An optimisation-based approach to reduce fuel consumption and emissions from shipping navigation

Ribeiro e Silva, S.[1,*] and Bento Moreira, M.[2]

ABSTRACT

This study presents an optimisation-based approach to reduce fuel consumption and emissions from shipping navigation. The main objective is to improve energy efficiency and simultaneously turn a case-study vessel compliant with Carbon Intensity Indicator (CII) proposed by IMO. This optimisation module has been devised as part of a new robust integrated real-time digital solution that will involve a significant number of both technical and operational measures in practice aiming to optimise operational efficiency (during navigation and port calls). Namely, the tool will be capable of situational awareness and decision support to reduce fuel consumption and Green House Gas (GHG) emissions from shipping and must be combined with intrinsic vessel systems to improve vessel hydrodynamic performance, resulting also in improved vessel safety and widening of the operational weather window.

KEY WORDS

Ship energy efficiency; Real-time fuel consumption estimation; Hydrodynamic optimisation; Weather routing; Vectorized simulated annealing.

INTRODUCTION

As the most energy efficient mode of transportation, the maritime transport sector is one of the major sectors of cargo shipping of goods around the world, but is also responsible for 681 [t] of $C0_2$ every year (see Hieminga and Luman (2023)). Hence, IMO is targeting a drastic reduction of Green House Gas (GHG) and $C0_2$ for shipping (see IMO (2023)). These ambitious targets involve major changes in the way ship owners, in general, and the maritime industry sector operates, bringing the need to adopt new technologies, investing in greener alternative fuels and adopting practical measures to improve current energy efficiency of the means of transportation.
In addition to this most challenging context of the maritime industry sector, many weather routing service providers claim the ability to save fuel and increase safety and schedule reliability. However, many seaman lives are frequently put at risk since more than 3,000 containers are lost overboard every year. According to the most recent report issued by the World Shipping Council ((see Larsson (2023)), the average annual loss for the two-year period 2020-2021 saw an increase to 3,113 from the 779 of the previous period, driven by major incidents. In 2020 the ONE Opus lost more than 1,800 containers in severe weather. The Maersk Essen also experienced severe weather in 2021 that resulted in the loss of some 750 containers. Also a study conducted by Gershanik (2011) revealed that weather routing helped to reduce ship rough weather damages by 73% and costs of maintenance and cargo damage law suits by 29% and 87%, respectively. At the same time the length of ship delays due to unfavourable weather reduced by 80% and fuel savings amounted to about 6%. With exaggerated capabilities and unsubstantiated benefits being advertised by weather routing companies, port authorities, ship owners,

[1] MARETEC (Department of Mechanical Engineering, Instituto Superior Tecnico, University of Lisbon, Portugal); ORCID: 0000-0003-0977-0629

[2] CENTEC (Centre for Marine Technology and Ocean Engineering, Instituto Superior Tecnico, University of Lisbon, Portugal); ORCID: 0000-0002-4948-6668

[*] Corresponding Author: ribeiro.e.silva@tecnico.ulisboa.pt

Submitted: 12 March 2024, Revised: 16 April 2024, Accepted: 1 May 2024, Published: 18 May 2024

Conference paper, DOI: https://doi.org/10.59490/imdc.2024.832 e-ISSN: 3050-4864

operators or charterers often face the difficult task of selecting the right service provider and level of technology suitable for their operations.
Anticipating that fuel prices in years to come will remain high due to war in Ukraine (see International Energy Association (2023)) and the conflict in the Middle-East plus the recent emphasis on reducing GHG emission in Europe, have resulted in renewed interest in further optimising ship performance. A recent DnV study (see DNV (2022)) indicated that while hydrodynamic performance (hull coating, hull form and trim optimisation and regular propeller cleaning) can achieve 5 to 15% reduction in fuel consumption and associated GHG emissions, more than 20% improvement can be achieved through technical and operational measures such as speed management, fleet planning and weather routing (the so-called logistics and digitalisation). Moreover, an experimental campaign conducted by HSVA with scaled models of a containership have demonstrated that hydrodynamic performance can be further improved in case an anti-rolling tank is installed to reduce ship motion waves (see HSVA (2020)).
To tackle the problem above, firstly, a numerical program has been developed at University of Lisbon, IST to evaluate added resistance in waves using output data of a standard strip theory seakeeping program developed by Ribeiro e Silva (2008). In this case, the strip theory code is based on Frank's Close-Fit method and the added resistance in waves is evaluated using the formulation originally proposed by Salvesen (1978). The program has provided good results against experimental data available in literature, especially for slender ship forms (see Ribeiro e Silva et al. (2011)). The numerical predictions presented in here have been compared against experimental data relative to ship's models with the same L/B ratio. Additionally, another Computational Fluid Dynamics (CFD) solver of the Navier-Stokes (N-S) type has been utilised to provide additional numerical predictions of the ship's total resistance in calm water and more detailed information on the flow characteristics around the ship's hull for distinct trim angles (see further details in Ribeiro e Silva and Eça (2024)).
More recently progressive increase in memory and speed of computers favours the utilisation of CFD N-S solvers, for current voyage planning purposes (i.e., simulations close to real-time for variable meteocen conditions) in conjunction with Salvasen method to predict added resistance in waves seems to be the most suitable decision support tool. Where a multi-dimensional (velocity and heading), multi-disciplinary constrained (rms ship motions and eventually with prevention of dynamic instabilities in waves), single objective (fuel consumption) optimisation algorithm has been proposed in order to take into account not only the pertinent fuel savings, but also the safety aspects of the voyage. Efforts have been focused so far on key technical-economic challenges that can demonstrate cost effectiveness and applicability of the concept. In particular, use of CFD simulations have been conducted with the aim of obtaining reliable predictions of calm water resistance, which combined with corrections for current, wind and wave effects lead to the development of this optimisation-based approach to reduce fuel consumption and emissions from shipping navigation.
Furthermore, development of a voyage planning module based on weather routing to save fuel and increase safety and schedule reliability (in terms of Just in Time arrival to port) has been envisaged. Hence, prior to integration of voyage planning module with the other Ship Operation Optimisation System (SOOS) modules and their full-scale demonstration during sea trials, all these modules must be extensively tested in a virtual environment to proper de-risk this new technology.
Firstly, the methodology used in this paper is presented in the Theoretical Background section, where an optimisation-based approach for enhanced fuel efficiency and safety aboard is described.
Secondly, in the Numerical Results section, some preliminary figures on the performance of the newly developed voyage planner are shown for a synthetic environment to demonstrate the capabilities of the tool. Namely, the range of surface currents, wind loading conditions and sea states which a typical containership usually operates in the Atlantic West coast of Portugal were simulated in order to set a numerical model that could be utilised to calculate the optimised fuel consumption for a desired average speed between two ports.
As mentioned in Conclusions, it is believed that calculation of specific hydrodynamic responses such as added resistance in waves for a real-time loading condition of the vessel, represents a major advantage in comparison with other commercial available tools, allowing as well the designer to define the most suitable hullform and superstructure area for the most energy efficient mode of operation of the vessel.

THEORETICAL BACKGROUND

In general, the hydrodynamic performance of a ship is influenced by the surrounding environmental conditions. In this context the existing space and time realizations of wind, waves and ocean current conditions can be defined as the environmental factors in any voyage. These factors will affect the fuel consumption by changing the power requirements for the propul-

sion of the vessel. Hence, this section attempts to presents a summary of the basic concepts in the realm of power estimates for the ship propulsion.

Power Curve Estimation

Ship's resistance is particularly influenced by the ship's hullform, speed, displacement and trim. In addition to these calm water parameters, added-resistance in waves or even wave-induced roll motion can also have a significant impact in the power delivered by the propeller. The total resistance R_T consists of several resistance components acting on the ship, which will be briefly describe in this section, while also referring to some relevant works that provide a more thorough and analytical presentation of methodologies to estimate those components of ship's resistance.
Hydrodynamic analysis for a specific hullform and ship loading condition can be used to calculate the components resistances acting on the ship by means of dimensionless resistance coefficients (see for example Harvald (1983)). This analysis may consist of using towing tank tests with scaled models, developing CFD models to simulate the flow around the ship, quasi-experimental methods using results of experiments and calculations. In case, calm water resistance is obtained, then seakeeping models can be utilised to estimate ship motions in irregular waves. In terms of CFD applications there are open source or commercial software that can be used in modelling ship resistance. In this study, CFD Simerics MP software considering a marine template to calculate ship resistance is used to determine calm water effective hull resistance at a given loading condition and range of ship speeds, i.e., the so-called power curve in calm water.
Calm water resistance is what a vessel would face in the event of total calm weather conditions, with an absolute lack of waves excluding the waves created by the ship moving in otherwise calm deep water condition. Calm water is very seldom encountered in real world conditions, particularly in ocean going voyages. For example, in the North Atlantic the probability of encountering calm water conditions is only 26 days in a year, i.e., 0.7%.
According to Scheekluth and Bertram (1998), calm water total resistance of a ship is made up of a number of different components, which are caused by a variety of hydrodynamic factors, and interact one with each other in a extremely complex way. Adopting a reductionist approach, calm water resistance consists of a viscous resistance plus the resistance due to the Kelvin waves generated by the hull. Viscous resistance is due to the viscosity of the water, which creates friction with the hull of the ship and depends, among other things such as the hull surface curvature, on the hull roughness and cleanness of the hull. With regard to the second component of calm water resistance component, wavemaking resistance, R_W, is closely associated with Kelvin wave system (i.e., waves generated from a moving pressure field with divergent and transverse systems). As it can be seen in Fig. 1, the wave system of a ship is composed of different Kelvin wave systems. Note that waves are generated by every point of the containership, where larger waves (more visible) are generated at the bow and stern.

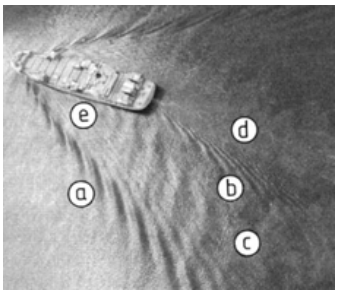

Figure 1: Different Kelvin wave systems of a typical containership, where: a) divergent bow wave; b) divergent stern wave; c) transverse wave; d) turbulent wake; e) quarter wave.

Ship calm water resistance, R_T, can be calculated as a function of the total resistance coefficient, $C_T = C_V(Rn)+C_R(Fn)$, the density of seawater, ρ_{sw}, the ship's speed over water, V_s, and the total wetted area of the hull, S_w, given by Eqn. (1).

$$R_T = \frac{1}{2}\rho_{sw} S_w V_s^2 C_T = \frac{1}{2}\rho_{sw} S_w V_s^2 (C_V + C_R) \tag{1}$$

Note that equation above is a simplified formulation of the complex nature of ship resistance in calm water, where viscous resistance coefficient, C_V, is assumed to be only dependent of Reynolds number (Rn), whereas the coefficient of residuary resistance, C_R, mainly composed by wavemaking resistance, C_W, is assumed to be dependent on Froude number (Fn). Once the main resistances have been estimated, it is possible to calculate the required effective power with appendages, P_{EA}, to move the ship through the water at the required sailing speed. Note that the effective power is simply the product of the total resistance times the speed over water, V_S. Based on that, the required nominal power at the main engine shaft (P_S) can be calculated using the shaft-line efficiencies, given by Eqn. (2).

$$P_S = \frac{P_{EA}}{PC} = \frac{R_{EA} V_S}{QPC \eta_S} = \frac{(R_T + R_{APP})\, V_S}{\eta_H \eta_O \eta_R \eta_S} \tag{2}$$

Hull efficiency, $\eta_H = \frac{P_{EA}}{P_T}$, is the ratio between the effective power with appendages and the power thrust, which depending on hydrodynamic pressure distribution around the hull, may attain values larger than 1.0. Open water propeller efficiency, $\eta_O = \frac{P_T}{P_{Do}}$, ranges approx. 0.60-0.75, whereas relative rotative efficiency, $\eta_D = \frac{P_{Do}}{P_D}$, of a conventional propeller ranges approx. 0.95-1.02. Note that power thrust (P_T) of the propeller is the power output that can be measured at thrust block bearing, whereas the open water delivered power or propeller power in open water (P_{Do}) is the power input measured during scaled model test of the propeller in open water, i.e., either towing tests or cavitation tunnel tests to measure thrust and torque developed by the rotating propeller without the presence of the ship's hull. Hence, propulsive coefficient (PC) can be calculated from quasi-propulsive coefficient (QPC) once shaft transmission efficiency is known, which is given by the ratio between delivered power with the propeller installed behind the hull (power measured at propeller flange) by power at the main engine shaft, i.e., $\eta_S = \frac{P_D}{P_S}$. Shaft transmission efficiency in conventional propulsion systems ranges 0.97-0.99 depending whether a simple or reversible reduction gearbox is intercalated in the shaft line or not (cases where 2-stroke low-speed diesel engine is installed).

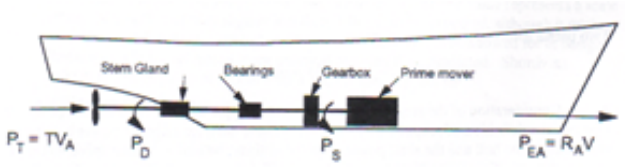

Figure 2: Different power and efficiencies along the shaft-line of a propulsion system, and locations where: a) effective power with appendages; b) shaft power; c) delivered power; d) thrust power can be measured.

As illustrated in Figs. 1 and 2, the behaviour of the flow around the hull determines the ship resistance and the wake at the propeller, which are interrelated. While the magnitude of the resistance directly determines the power requirements, the magnitude of the wake and its distribution at the propeller plane also affects the power requirements as well as the performance characteristics. When the wake distribution is highly non-uniform at the propeller plane, this is a major source of poor propulsive efficiency (η_R), cavitation, vibration and noise. Assuming some simplifications, the main engine that satisfies the propeller's demands, and allows the ship to sail at its nominal speed during voyage, can be selected. Note that this main engine rated power should cover the propulsion demands considering as well an appropriate power margin that will depend on certain cost elements (acquiring, operating and maintenance), reliability and adaptability to different operating patterns of the vessel.

Wind Resistance

In first place, it is recalled that wind is the cause to the creation of waves so that their incoming direction is sometimes practically the same, and simultaneously wind acts as a force on the vessel known as wind resistance. Wind resistance will affect all surfaces of the ship above the sea-surface as well as cargo when the latter is above the hull, as it is the case of most containerships. According to Bernoulli's equation, wind resistance either in the x or y direction is directly proportional to the projected transverse cross-sectional (A_T) or lateral (A_L) areas of the ship above the waterline, the density of the air,

ρ_{air}, and the square of the wind speed. These two projected areas are defined by the above-water part of the main hull and any superstructures (e.g., cargo, bridge, funnel, and equipment). Normally wind represents around 2% of the total resistance, with the notable exception of containerships where due to both large projected transverse cross-sectional and lateral areas of the vessel (due to 60% of containers on-board are pilled-up above main deck) the contribution can reach up to 10%.

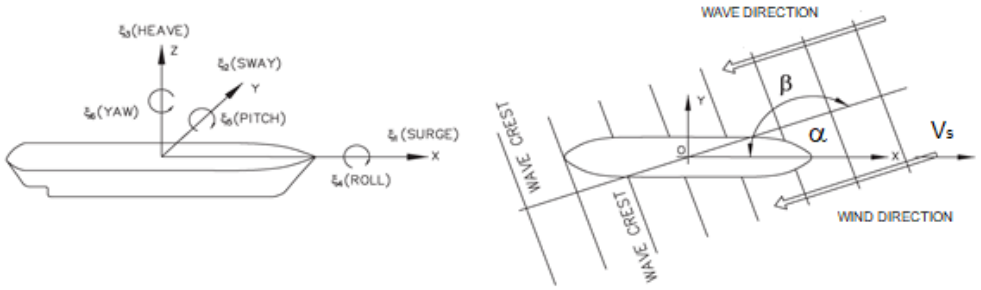

Figure 3: The non-inertial body-fixed tri-axial coordinate system of the ship, illustrating the six modes of motion and the definition of the true wind vector (α) and wave (β) incoming direction angles.

The wind force is typically divided into two components: the fair wind, which is what the ship is facing during sailing (same speed but opposite direction of the vessel), and the true wind, which is the actual wind speed and direction at the current position at sea. The former can be computed using either a semi-empirical formulation proposed by Gould (1982) or a standard CFD tool Ribeiro e Silva and Eça (2024) and is essentially the wind that the vessel would face due to the fact it is sailing, while the latter would be the wind the vessel would face at the same location if she was anchored. Adding these two vector components, the resulting apparent wind vector can then be used to calculate the total wind resistance. As illustrated in Fig. 3, the true wind induced longitudinal and transverse force components and the yawing moment can be calculated using the following equations originally derived by Isherwood (1972),Gould (1982) and Blendermann (1994):

$$\begin{bmatrix} F_{wx} \\ F_{wy} \\ M_w \end{bmatrix} = \frac{1}{2}\rho_{air} V_w^2 \begin{bmatrix} C_{wx}\left(\alpha_w\right) A_T \\ C_{wy}\left(\alpha_w\right) A_L \\ C_w\left(\alpha_w\right) x_{wc} \end{bmatrix}, \tag{3}$$

where x_{wc} represents the distance between the center of the lateral area of the ship above waterline and midships and the force components are given by Eqns. (4) and (5):

$$F_{wx}\left(\alpha_w\right) = F_w\left(\alpha_w\right)\cos\left(\alpha_w\right) \tag{4}$$

$$F_{wy}\left(\alpha_w\right) = F_w\left(\alpha_w\right)\sin\left(\alpha_w\right) \tag{5}$$

Assuming that wind force Cartesian components in surge and sway are expressed by $F_{wx}(0°)$ and $F_{wy}(0°)$, respectively, then the resulting true wind induced force at any given incoming angle, α_w, may be expressed as:

$$F_w\left(\alpha_w\right) = F_{wy}\left(90°\right)\left\{\frac{2\sin^2\left(\alpha_w\right)}{1+\sin^2\left(\alpha_w\right)}\right\} + F_{wy}\left(0°\right)\left\{\frac{2\cos^2\left(\alpha_w\right)}{1+\cos^2\left(\alpha_w\right)}\right\} \tag{6}$$

Note that more precise wind load calculations could have been performed to take into account as well a given vertical wind profile. In this case, an effective wind speed and the lateral center of pressure for a gradient wind could be also estimated by

subdividing the frontal and lateral projections into small elements so that after surface integrals have been conducted new non-dimensional wind load coefficients $C_{wx}(\alpha_w)$, $C_{wy}(\alpha_w)$ and $C_w(\alpha_w)$ could be obtained.

Added-Resistance in Waves

Both involuntary and voluntary speed reductions are taken into account to avoid over-predicted ship speed and wrong diversion decisions when facing rough weather, not to mention inaccurate estimates of fuel consumption and time of arrival. To prevent this problem, added-resistance in waves for a specific loading condition and a given hullform will be computed as well using a state-of-the art numerical tool. Note that this additional component of resistance called added-resistance in waves, R_{aw}, is heavily non-linear. In fact, estimating added resistance is a complex process, as this generally depends on hullform, hydrodynamic characteristics of the ship and the encountered sea spectrum. For the calculation of the added resistance in waves, Salvesen 1978 method using strip theory approximation has been adopted. In this case, the strip theory code is based on Frank's Close-Fit method and the added resistance in waves is evaluated using the formulation originally proposed by Salvesen plus a correction for short waves. Hence, using this strip theory, Salvesen introduce the added-resistance in waves, given by Eqn. (7):

$$R_{aw} = -\frac{1}{2} k \cos\beta \sum_{j=3,5} \zeta_k \left\{ \left(F_j^I\right)^* + \hat{F}_j^D \right\} + R_7, \tag{7}$$

where $(F_j^I)^*$ is the Froude-Krylov force and moment, $(F_j^D)^*$ is the diffraction force and moment, R_7 is the added-resistance due to diffraction potential, ζ_k is the ship's displacement induced by waves in k direction.
In case head waves scenario is considered, in this study, the equation can be more conveniently expressed as Eqn. (8):

$$R_{aw} = \frac{i}{2} k \left\{ \zeta_3 \hat{F}_3 + \zeta_5 \hat{F}_5 \right\} + R_7, \tag{8}$$

where the incident and diffracted components are given by Eqn. (9):

$$\hat{F}_j = \left(F_j^I\right)^* + \hat{F}_j^D \tag{9}$$

The complex amplitude for the incident wave potential for head waves having wave amplitude ζ_w^a and angular frequency ω can be expressed by Eqn. (10).

$$\phi_0 = \frac{ig\zeta_w^a}{\omega} e^{ikx+kz} \tag{10}$$

Hence, heave components of added-resistance in waves are given by Eqn. (11):

$$\hat{F}_3 = \zeta_w^a \int_L e^{-ikx} e^{-kds} \left\{ \rho g b - \omega_e \left(\omega a_{33} - i b_{33} \right) \right\} dx, \tag{11}$$

and pitch components of added-resistance in waves are given by Eqn. (12):

$$\hat{F}_5 = -\zeta_w^a \int_L e^{-ikx} e^{-kds} \left\{ \rho g b - \omega_e \left(x + \frac{iV_S}{\omega} \right) \left(\omega a_{33} - i b_{33} \right) \right\} dx, \tag{12}$$

where $d =$ sectional draft, $s =$ sectional area coefficient, $b =$ sectional breadth, $\omega_e = \omega - \frac{\omega^2}{g} V_S cos\beta =$ encountering wave frequency, $a_{33} =$ sectional heave added mass coefficient and $b_{33} =$ sectional heave damping coefficient.
Added-resistance due to diffraction potential can be expressed as Eqn. (13) for calculating head sea result:

$$R_7 = \frac{i}{2} \left(\zeta_w^a\right)^2 k \frac{\omega_e^2}{\omega} \int_L e^{-2kds} b_{33} dx \tag{13}$$

Note that a non-dimensional added-resistance in waves can then be simply defined by the summation of the three dimensional components $R_{aw} = \hat{F}_3 + \hat{F}_5 + R_7$ as:

$$R'_{aw} = \frac{\hat{F}_3 + \hat{F}_5 + R_7}{\rho_{sw} g \left(\frac{B^2}{L_{pp}}\right) \left(\zeta_w^a\right)^2} \tag{14}$$

Next, a practical simplification can be introduced to estimate added-resistance in waves directly from head sea result, where added-resistance in waves at any angle β relatively to head waves is given by Eqn. (15):

$$R_{aw}\left(H_S, T_P, \beta\right) = R_{aw_{180^\circ}}\left(T_P\right) \left(\frac{H_S}{2}\right) \cos^2 \beta \tag{15}$$

Trim Effect on Ship Resistance

CFD with RANS turbulence models can address a wide variety of flows including external flows around bodies of a certain shape, i.e., statistically steady flows that require streamlined shapes aligned with the incoming flow where boundary-layers do not exhibit significant flow separation. However, for trim optimisation these simulations must be supported by relevant background experience in the realm of CFD tools utilisation and must be subjected to a dedicated Verifcation and Validtion (V&V) procedure.

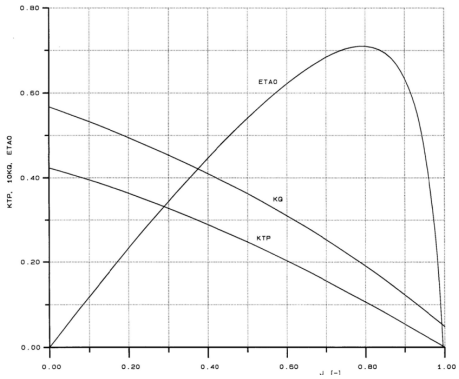

Figure 4: Schiffbau Versuchsanstalt Potsdam GmbH: Open-water propeller test diagram of a variable pitch propeller (VP 1124)

.

CFD simulations of ship performance in waves will be mainly built around an advanced actuator disk model implemented either in or Simerics MP, which reads the open water performance of a real propeller (see Fig. 4). Notice should be given to the fact that being able to remove the actual propeller geometry from the numerical computations considerably simplifies the physics and speeds up the process. Moreover, experimental results from scaled model testing or sea trials having sys-

tematic draught and trim variations are expected to be compared and contrasted against CFD simulation results in the near future.
Firstly, considering the geometry of the hull, accurate ideal trim predictions of the total CFD resistance in calm water must be determined for enhanced stability and fuel consumption optimisation purposes. Secondly, the vessel floatation, and the corresponding flow characteristics at the propeller plane during operation must be optimised to attain the least required power solution for a specific design loading condition by means of altering the vessel's position of centre of gravity of the ship, $CG(x, y, z)$. Note that instantaneous location of the center of gravity of the ship, $CG(x, y, z, t)$ depends on magnitude and location of a large number N of i discrete weights aboard, including fuel and ballast water in the aft and peak tanks, is given by:

$$CG\left(x, y, z, t\right) = \frac{\sum_{i=1}^{N}\left[m_i\left(t\right) \times \left(x_i, y_i, z_i\right)\right]}{\sum_{i=1}^{N} m_1\left(t\right)} = \frac{M_i\left(x, y, z, t\right)}{\Delta\left(t\right)} \tag{16}$$

Next, using one particular hydrostatic parameter called unit moment to change trim (M_U), the required instantaneous trim angle variation, $\delta\theta(t)$, for enhanced stability and fuel consumption optimisation purposes can be easily calculated by SOOS from the instantaneous variation in the longitudinal inclining moment, $\delta M_I(x, t)$, using the Eqn. (17):

$$\delta\theta(t) = \frac{\delta M_I(x, t)}{M_U} \tag{17}$$

Finally, added-resistance in waves component for this particular new loading condition as well as wave induced roll motion component of total ship's resistance will be computed in the near future using SOOS.

Vectorized Simulated Annealing (VSA)

Fuel consumption C while sailing from points A to B, depends on the route L chosen and can be computed using the following line integral with respect to the arc length:

$$C = \int_L \frac{\frac{\partial M}{\partial t}}{V} ds, \tag{18}$$

where $\frac{\partial M}{\partial t}$ and V stands respectively for fuel consumption time rate and the speed along L. Note that $\frac{\partial M}{\partial t}$ and V depends particularly on environmental conditions such as wind, currents and waves. Therefore, the route that minimizes global fuel consumption, in such conditions, is not the straight (or geodesic) path from A to B.
The approach that has been adopted to find the route L that minimizes the global fuel consumption is the Vectorized Simulated Annealing (VSA) technique which is based on the Simulated Annealing (SA) method, see Press (2007). This method can be roughly described using the analogy with the metallurgical process of annealing to bring a metal from an high energy/temperature state to a crystal lattice state of minimum/temperature energy. At a high temperature, the different elements that characterize the system register significant variations in their respective positions, resulting from their high kinetic energy. As the temperature decreases, the system assumes lower energy and more stable configurations and the changes in position of the system's constituents occur with a smaller amplitude. In case the temperature decrease is not too rapid and if during it the system has the possibility of assuming less probable configurations (of higher energy), the retention of the system in meta-stable configurations will be less likely. A slow and gradual decrease in temperature will allow the system to properly explore the search space and assume the configuration of minimum energy by the end of the annealing process. SA method was developed by Metropolis and co-workers, see Metropolis et al. (1953). A comprehensive description of this method, also known as the Metropolis-Hastings algorithm, can be found in Hitchcock (2003). The VSA method applies components of the SA algorithm in parallel to a population of systems that constitute the components of a vector. This methodology has been successfully applied in previous works such as Maurício and Moreira (2022).

In the application of the VSA method, paths will be modelled by a process of proper concatenating oriented segments. Note that any path between A and B can be arbitrarily approximated in the aforementioned manner. So, define N concatenated oriented segments L_i(legs) that establish a route L between points A and B. This path is thus defined by $N-1$ yaw points P_i. The global fuel consumption C in L is given by:

$$C\left(L\right)=\sum_{i=1}^{N}C\left(L_i\right), \tag{19}$$

where $C\left(L_i\right)$ is the fuel consumption in leg L_i.

Note that Eqn. (19) can be numerically integrated (with respect the arc length) using a standard numerical integration method (e.g., trapezoidal rule) and adopting an appropriate spatial discretization of the leg over the corresponding leg L_i.

$$C\left(L_i\right)=\int_{L_i}\frac{\frac{\partial M}{\partial t}}{V}ds \tag{20}$$

The aim is to determine the positions of the yaw points P_i thus determining the path L that minimize the global fuel consumption C. As previously mentioned, fuel consumption rate $\frac{\partial M}{\partial t}=\frac{\partial M}{\partial t}\left(x,y\right)$ and speed $V=V\left(x,y\right)$ along the routes depend on environmental conditions.
Note that (x,y) stand for the spatial coordinates. The estimation of the fuel consumption time rate will consider the effect of wind (intensity and direction), the resistance associated with waves (significant height, period, and direction), and the effect of drift produced by currents. Later on consideration of the effects of roll motion in formulating this fuel consumption optimisation problem will be considered.

VSA NUMERICAL MODELLING

Main details in the implementation of the heuristic to minimize Eqn. (18) comprises five main steps as follows:

(i) Generate a set U, of $2M$ different routes L^j from A to B, each one defined by sequences of $N-1$ yaw points in randomly distributed spatial positions;

(ii) Compute de fuel consumption $C\left(L^j\right)$ on each one of the routes in U and retain an ordered subset $V\subset U$ of the routes with the lower global fuel consumption. Typically $\#V=\frac{\#U}{2}$. Note that routes L^j, in

$$V=\left\{L^1,L^2,\ldots,L^j,\ldots,L^k,\ldots,L^M\right\},$$

must be ordered such that $C\left(L^j\right)<C\left(L^k\right)\Rightarrow j<k$;

(iii) Construct a new set U concatenating a new set of V with previous set of best performers V and apply a randomly uniformly distributed $2-D$ spatial perturbation of maximum semi-amplitude ε to the positions of each one of the yaw points that define each of the $2M-1$ last routes in U. The first and better route in the current epoch remain undisturbed and survive to integrate the set U in the next epoch without any perturbation imposed in order to prevent that a top performer candidate prematurely detected could be discarded;

(iv) Repeat steps $(ii)-(iii)$ using in each repetition a smaller semi-amplitude ε of the maximum spatial perturbation;

(v) Stop when the best route in V route fails to show significant improvements or, after P repetitions.

Note that the successive repetition of steps $(ii)-(iv)$ allows us to define a sequence $U\left(i\right)$, $i=1,\ldots,P$ of route sets and a related sequence $\varepsilon=\varepsilon(i)$, $i=1,\ldots,n,\ldots,P$ of maximum semi-amplitude spatial perturbation of the yaw points, where

each i define an "*epoch*". Moreover, $\varepsilon = \varepsilon(i)$, $i = 1, \ldots, n, \ldots$, must be a slowly decreasing function in order to ensure an adequate survey of the search space. In particular, the slow decreasing negative exponential function given by the Eqn. (21) can be used:

$$\varepsilon\left(i\right) = d \times e^{-\sigma \times i}, \tag{21}$$

where d stands for a characteristic length, related with the distance from A to B, for instance. The decreasing coefficient σ is given by Eqn. (22):

$$\sigma = \frac{\ln\left(\frac{d}{\delta}\right)}{P}, \tag{22}$$

where δ is small residual distance and P is the global number of epochs. Note that when $i = P$, the following detection is obtained:

$$\varepsilon\left(P\right) = \delta, \tag{23}$$

which means that δ and P must be selected assuring the decrease of ε is slow enough and the spatial perturbations of the position of the yaw points of semi-amplitude of δ will be irrelevant.
Before real-data is utilised, a synthetic environment has been proposed to obtain preliminary checks on performance of this decision-support tool. After these V&V studies, the newly developed voyage planner must be compared and contrasted with available sea-trials results.

NUMERICAL RESULTS

In this section the numerical results of a fully integrated voyage planner for enhanced fuel efficiency and safety aboard a 712 TEU geared containership (see Appendix) are presented. Firstly, a synthetic environment is utilised to check consistency of the fuel consumption results under three scenarios: (i) ocean currents, (ii) wind loads and (iii) wave conditions. Moreover, navigation interdiction zones such as traffic corridors or islands have been introduced to check consistency of the optimisation-based approach to reduce fuel consumption and emissions from shipping navigation.
Finally, using a scenario of real-case meteocean conditions for a given geographical area (obtained from the numerical model MOHID) still in a synthetic environment, some preliminary figures on the performance of the newly developed voyage planner in terms of fuel consumption reduction can be obtained. Note that MOHID is a large circulation hydrodynamic model able to provide either hindcast or forecast predictions of wind, waves, and currents for distinct design-points, i.e., either small domestic routes or long hauls (transoceanic crossings).

Calm Water Power Estimation

As shown in Figs. 5 and 6, the power curve [knots versus kW], can be modelled by means of a 3rd order polynomial fit of the type $f(x) = a_3x^3 + a_2x^2 + a_1x + a_0$, where the coefficients of this polynomial obtained by means of linear regression reads $a_2 = -0.275$, $a_3 = 6.510$, and $a_1 = a_0 = 0.0$. Note that the polynomial function obtained must be equal to zero at the origin so that effective power will be extinct at ship's zero speed ($a_0 = 0.0$). Moreover, a second condition has been imposed to this polynomial fit of the effective power in terms of having also zero resistance at zero speed, so that at the slope of the effective power at the origin must be also zero, i.e., $dP_E/dV_s = 0.0$ at $V_s = 0$ implying additionally that $a_1 = 0.0$.

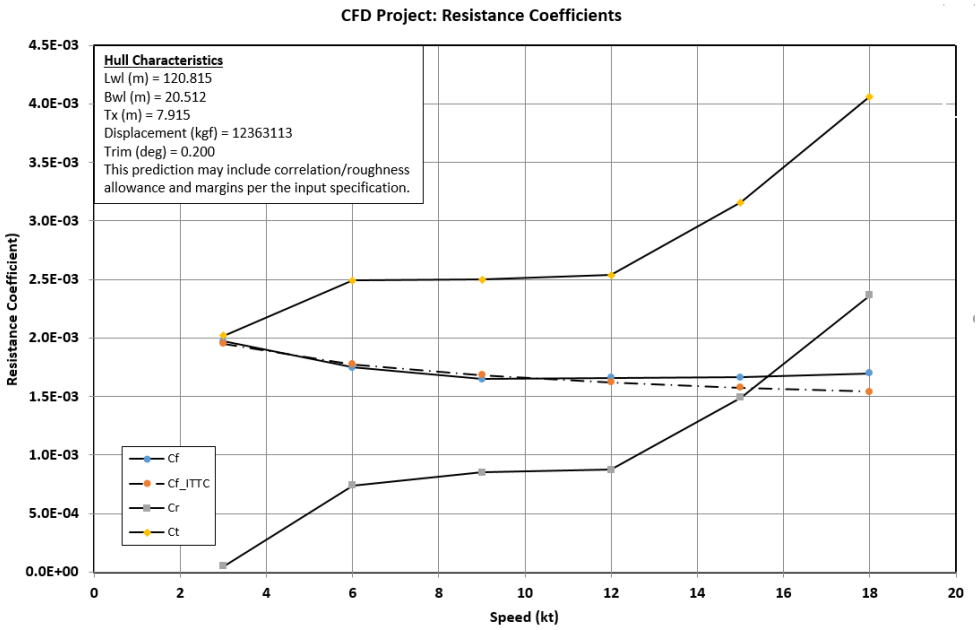

Figure 5: CFD resistance coefficients in calm water from Simerics MP of the containership

.

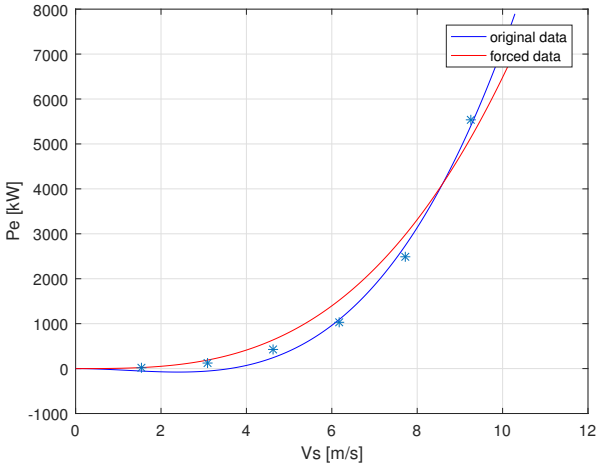

Figure 6: Power curve in calm water of the containership [m/s versus kW]

.

Finally, to prevent the power curve to take negative values at low speeds (see Fig. 5) a third local condition has been imposed to force the polynomial to move upwards by means of introduction of an extra point located upwards. This extra point that can be interpreted as an outlier point, whose magnitude is large enough to obtain a forced power curve always positive (see forced data curve of Fig. (6) coloured in red).
From the rated power of the CFD effective power curve at an ideal trim of $\theta = 0.2^o$ by the stern, a propulsive coefficient of the containership at top speed of $PC = 0.656$ has been determined.

Wind Loads Estimation

Firstly, estimation of forces (and moments) caused by wind resistance have been conducted for the containership facing head and beam winds. Next, as shown in Fig. (7), trigonometric relations given by Eqn. (3) can be used to determine the wind loads coefficients at different incoming angles of direction of the wind relatively to the ship's heading.

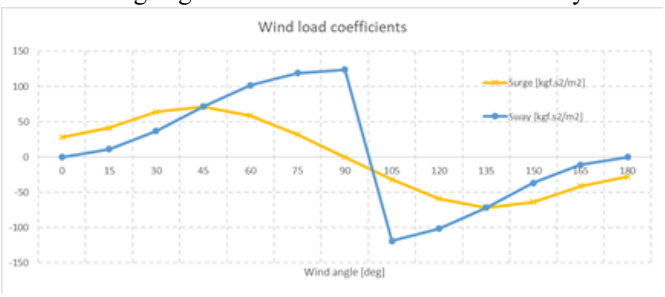

Figure 7: Wind load coefficients in surge and sway of the containership

.

Note that instead of using Gould's semi-empirical formulation, a more accurate assessment of the impact of wind on this containership could have been conducted by means of CFD. In that case, CFD presents many advantages, of which the most obvious is adequacy for flow visualization and for design optimisation of all surfaces of the ship above the sea-surface as well as cargo. However, proper selection of the choice of the CFD method as well as a grid convergence study should be adopted in first place to prevent results become affected by the mesh and input data selection. Hence, in this preliminary study a faster methodology has been adopted for demonstration purposes.

Added Resistance in Waves and Speed Loss Estimation

As shown in Figs. (8) and (9), there is a fair agreement between Salvesen (1978) and Gerritsma and Beukelman (1979) numerical predictions of added resistance in head waves. In close or open quartering waves the added resistance curves obtained by Gerritsma&Beukelman (1979) present larger deviations and in the opposite direction practical experience of the authors as seafarers, therefore Salvesen (1978) is considered to provide more accurate predictions when compared with experiments, so that this will be the adopted methodology in this study.

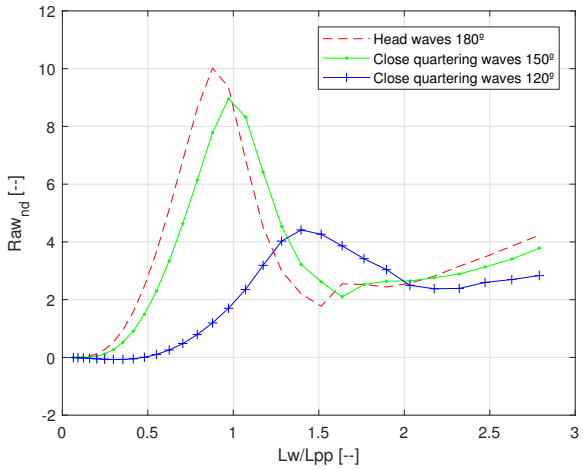

Figure 8: Transfer functions of non-dimensional added resistance in wave ($R_{aw} = R_{aw}/(\rho_{sw} g B^2/L_{pp}\zeta_w^{a\,2})$ versus ratio of wave to ship's length between perpendiculars (λ_w/L_{pp}) in head waves (180^o in red dashed line), close quartering waves (150^o in green line) and open quartering waves (120^o in blue line with cross) of the containership at top speed, calculated by the Salvesen, 1978 method

.

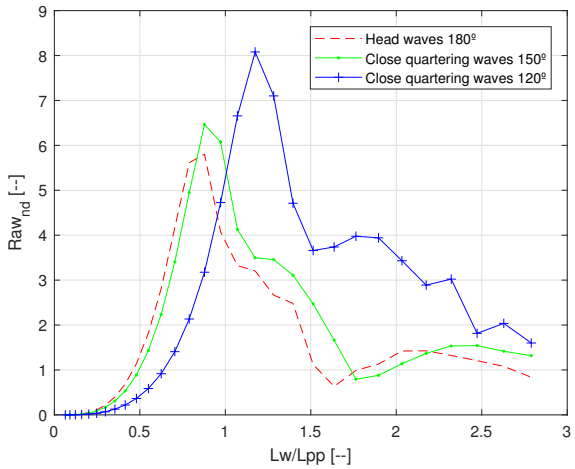

Figure 9: Transfer functions of non-dimensional added resistance in wave ($R'_{aw} = R_{aw}/(\rho_{sw} g B^2/L_{pp})\zeta_w^{a\,2}$) versus ratio of wave to ship's length between perpendiculars (λ_w/L_{pp}) in head waves (180^o in red dashed line), close quartering waves (150^o in green line) and open quartering waves (120^o in blue line with cross) of the containership at top speed, calculated by by Gerritsma&Beukelman, 1979 method

.

Non-dimensional added resistance in waves estimates versus wave frequency for top speed ($Fn = 0.26$) are shown in Figs. (8) and (9). Next, considering the design-point peak wave period and wave height along with Eqn. (15) the added resistance in waves for any wave condition encountered at sea with a certain relative incoming wave direction can be easily calculated. For example, considering the containership is facing the most statistically frequent wave train with a peak period around $T_P = 9$ [s] and a significant wave height of $H_S = 1.25$ [m], the resulting added resistance in head waves is 13.42 [kN], which represents 1.7% of the total resistance or 2.9% of the residuary resistance at top speed.

Weather Routing Assumptions

Considering the effect of environmental conditions in the ship's resistance in otherwise calm water. Namely: wind, waves and ocean currents. The present implementation of VSA allows to find the route that minimizes global fuel consumption under the influence of these most relevant environmental conditions. Notice should be given to the fact that, at this initial stage, either synthetically generated or MOHID predicted environmental conditions are assumed to be steady, so that preliminarily testing of the developed algorithms and the proposed heuristic can be conducted via numerical simulations.
The encoding of land presence and prohibited passage zones (e.g., marine traffic corridors) has been also added to the heuristic with the aim of equipping SOOS to handle such unavoidable and common restrictions in determining a realistic route. Programming this functionality involves assuming a practically zero speed of the ship in land or prohibited zones.
The trajectory from point A to B is planned to be carried out at a ship's advance base speed V_0 to reach the destination within the estimated or desired time. At this stage of the development of SOOS, the estimation of the effects of wind, waves, and ocean currents on speed and fuel consumption involved the formulation of some simplifications, namely:

(i) In considering the effects of environmental conditions, the principle of superposition will be applied, i.e., implicitly linearity in the dynamic behaviour of the system in the neighbourhood of V_0 and C_0 is assumed . Hence, the variation (either increase or decrease) in speed or fuel consumption stemming from environmental conditions will simply be added to the base velocity V_0 and the base fuel consumption C_0.

(ii) In the calculation of wind, drift, and current effects it has been assumed that vessel's heading is equal to her course;

(iii) Vessel drifting associated with wind loads has been neglected, and the wind loads will only impact the increased or decreased resistance to ship's advance. Consequently, leeway corresponds only to either increments or decrements to the base consumption C_0. The increased or decreased resistance to ship's advance is computed using the formalism condensed in Eqn. (4);

(iv) The increases or decreases in speed along the course caused by ocean currents at the free-surface will simply be added to the ship's advance base velocity V_0. The leeway produced by ocean currents will be considered only as an increase in the base consumption C_0, i.e., the corresponding increase in the velocity to maintain the ship's advance base velocity V_0 along the defined course over ground;

(v) Waves will be characterised by significant wave height, H_S, spectral peak period, T_P, and a relative incoming incidence angle, β, which will induce an additional ship's resistance component. This ship's resistance component will be varying from a maximum to zero depending on a spreading function, which is defined by an incidence angle in the range $-\frac{\pi}{2} \leq \beta \leq \frac{\pi}{2}$ radians, using the formalism exposed in Eqn. (15).

In the absence of wind, waves, and currents, let P be the power required to maintain speed V, let R be the resistance offered by the water and air to the displacement of the ship at speed V, and let C be the corresponding fuel consumption time rate, it has been assumed that:

$$P = a_1 V^2 + a_2 V^3, \tag{24}$$

$$R = a_1 V + a_2 V^2, \tag{25}$$

and

$$C = k\left(a_1 V^2 + a_2 V^3\right), \tag{26}$$

where k, a_1 and a_2 are fitting coefficients to be computed from previously obtained using CFD or empirical data.

Combining Eqns. (25) and (26) it is obtained:

$$\triangle C \approx \frac{k\left(2a_1 + 3a_2V_0\right)V_0}{\left(a_1 + 2a_2V_0\right)}\triangle R, \tag{27}$$

and

$$\triangle C \approx k\left(2a_1V_0 + 3a_2V_0^2\right)\triangle V. \tag{28}$$

These expressions will be used to estimate the consumption increments, $\triangle C$, associated with the computed increases in resistance, $\triangle R$, and velocity, $\triangle V$, resulting from the effects of the above mentioned considered environmental conditions. It should be stressed that linearity in the dynamic behaviour of the system in the neighbourhood of V_0, has been assumed, so that the present formulation will only be valid in a context where the effects of wave wind and currents are sufficiently moderate.
At a later stage of this work, the results will be experimentally validated by means of sea-trials, so that simplifications made in the formalism used in here might be appropriately adjusted.
In the implementation of the VSA technique, synthetic environmental conditions have been defined in an appropriate spatial grid. Namely, a non-uniform wind velocity field having a maximum wind speed of approximately 23 [kts], an uniform ocean current of 2.14 [kts] with direction 270^o and an uniform field of regular waves with direction 270^o characterized by a significant wave height H_S of 1.25 [m] and period T_P of 10 [s] has been adopted. The starting point A, with Cartesian coordinates: $(x_A, y_A) = (-100, 70)$ and the destination point B with coordinates: $(x_B, y_B) = (100, -10)$ were also defined. Note these points were only approximately 215 [m] apart from each other to speed up the process.

The power curve (P in [kW] and V in [m/s]), given by: $P = a_1V^2 + a_2V^3$, and the fuel consumption time rate curve (C in [kg/s]), given by: $C = k\left(a_1V^2 + a_2V^3\right)$, used in the simulations where characterized by the following parameters:

Table 1: Parameters defining the power and the fuel consumption time rate curves.

a_1	-0.275
a_2	6.510
k	$5.069\,4 \times 10^{-5}$

The minimal global fuel consumption route was defined by 5 yaw points and the heuristic was executed in a set U with 200 routes evolving over 750 epochs.
In Fig. 10 the evolution of minimum global fuel consumption from epoch to epoch is shown. Also, the corresponding determination of the optimal path is represented in Figure 11. Notice should be given to the fact that in this particular simulation less than 100 epochs were necessary to obtain the minimal route.

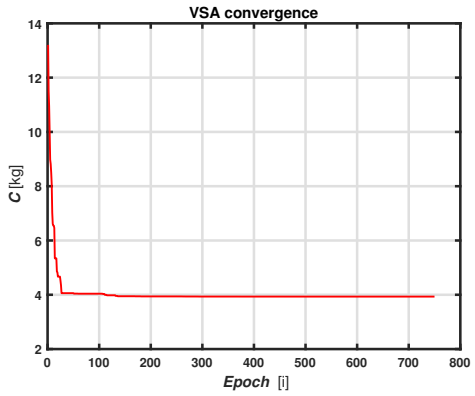

Figure 10: Evolution of minimum global fuel consumption from epoch to epoch.

In Fig. 11 results provided by the heuristic under the aforementioned conditions are shown. It can be observed that minimal route exhibits a lower global fuel consumption than the global fuel consumption associated with the direct route. Actually, the fuel savings observed in the minimal route determined are, approximately, 9% with respect to the fuel consumed in the direct route, which is considered quite promising at the fuel prices nowadays.

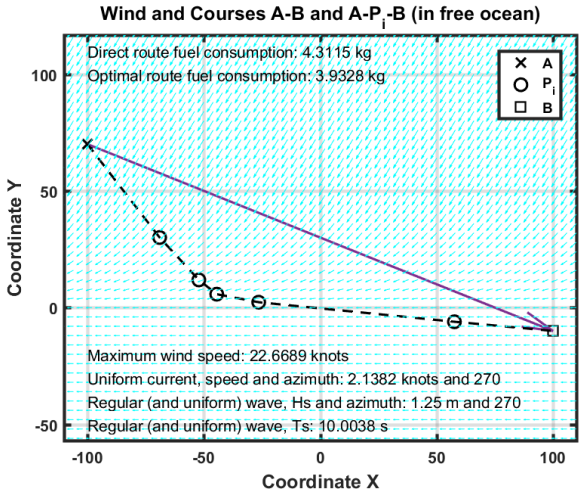

Figure 11: Minimal route from A to B in free ocean.

As illustrated in Fig. 12, all the simulation conditions remained unchanged, an exception being made for the addition of an ”island” to the original grid in an exact location corresponding to the passage zone of the minimal route represented in Fig. 11. In this new situation, as expected, the minimal route determined circumvents the island. Despite this change, the new determined route still allows for a fuel saving of approximately 8%, compared to the global fuel consumption over the direct route.

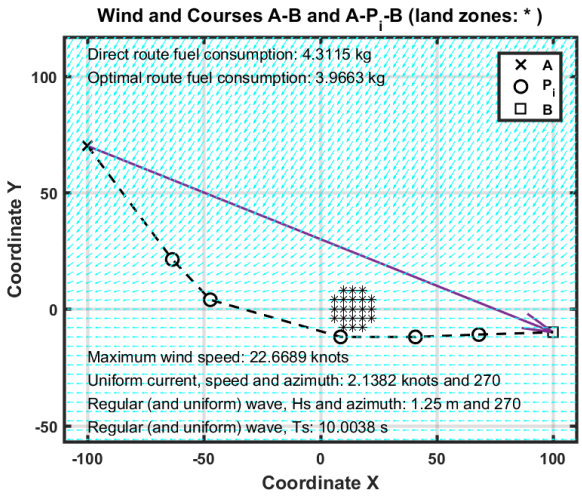

Figure 12: Minimal route from points A to B with land zones.

The simulation results are considered very satisfactory and highlight the potential of the developing application. The results obtained so far demonstrate that a rational weather routing is conducive to an increase in ship safety and energy efficiency. In fact, from these numerical simulations, the fuel consumption of a given voyage can be significantly reduced to 9% or 8% (see ratios of fuel consumed between optimal and direct route shown in Figs. 11 and 12). At the same time, fuel consumption reduction will create the double benefits of reducing the cost of ship operations while also reducing engine gas emissions that come from burning extra fuel, i.e., making the vessel compliant with new CII regulations proposed by IMO. In the near future, more simulations will be conducted with realistic environmental forecasts provided by a large circulation hydrodynamic model, such as MOHID (see (Neves, 1985)).

CONCLUSIONS AND FUTURE WORK

In this study the development of an optimisation-based approach to reduce fuel consumption and emissions from shipping navigation has been presented. The current study demonstrates that hydrodynamic performance can be substantially improved by means of trim optimisation that allows ships to reduce fuel consumption and simultaneously operate in adverse weather conditions with minimum degradation of their mission effectiveness.

Firstly, from a set of synthetic environments some preliminary figures on the performance of this newly developed voyage planner based on Vectorized Simulated Annealing (VSA) method was assessed in terms of fuel consumption as a function of speed over ground due to ocean currents and wind loads. Next, the assessment of added-resistance in waves induced by local wave conditions was introduced still as a synthetic environment to check consistency of the fuel consumption results. The simulation results are considered very satisfactory and highlight the potential of the developing a practical application where land zones or traffic corridors are taken into consideration. Actually, the fuel savings observed in the minimal route determined are, approximately, 9% with respect to the fuel consumed in the direct route, which is considered quite promising at the fuel prices nowadays.

In the near future, using a real-case environment scenario the performance of the Ship Operation Optimisation System (SOOS) in terms of fuel consumption reduction along with its comparison with other commercial available tools will be obtained. Moreover, next results are expected to allow the containership operator to have confidence that this containership after mid-life refit to convert an existing anti-heeling tank into an anti-rolling U-type tank will be capable of meeting and in some cases exceeding their operational requirements in terms of energy efficiency due to its superior hydrodynamic performance in a real scenario sea conditions. Contrarily to other decision-support tools systems, SOOS will provide enhanced energy efficiency and roll stabilisation at zero as well as at any advance speed. Therefore, SOOS will be a very attractive option for vessels performing operations that require a large range of speeds. Moreover, the objective of describing the selection process of the most appropriate decision-support tool and roll stabilisation system at the ship's life cycle will be also

achieved.
Looking ahead, there is a significant potential for innovation in this field of providing the maritime transport sector with customised decision-support systems, and further applied R&D is necessary to develop this potential. This is reinforced by current trends toward increased automation and reduced manning of maritime operations and the regulation requirements in the European context.

DECLARATION OF GENERATIVE AI AND AI-ASSISTED TECHNOLOGIES IN WRTITING

Statement: During the preparation of this work the author(s) have not used generative AI neither AI-Assisted Technologies in writing.

CONTRIBUTION STATEMENT

Author 1: SOOS conceptualization; supervision; MOHID hydrodynamic model data curation; methodology; CFD simulations of ship's resistance in calm water; Strip theory method calculations of hydrodynamic coefficients in FORTRAN; Salvesen (1978) and Gerritsma&Beukelman (1979)'s added resistance and roll motion responses in waves modules programming in MatLab; writing – original draft, review and editing. **Author 2:** VSA conceptualization; Synthetic model data curation; VSA module programming in MatLab; writing – original draft, review and editing.

ACKNOWLEDGEMENTS

This work was partially funded trough MARETEC project ASTRIIS (Atlantic Sustainability Through remote and In-situ Integrated Solutions), where a large group of partners (Tekever Space, CoLAB +ATLANTIC, CEiiA - Centro de Engenharia e Desenvolvimento, IST, Abyssal S.A., Hidromod, Spinworks, ISQ, WavEC, Universidade do Algarve, Universidade do Minho, Faculdade de Engenharia do Universidade do Porto, Oceanscan) aims to develop an Autonomous Surface Vehicle for Search and Rescue (SaR) along with a scalable tool for simulation and training of SaR operations (with a sustainable business model) using an high-fidelity immersive virtual marine environment.

REFERENCES

Blendermann, W. (1994). Parameter identification of wind loads on ships. *J. Wind Eng. Ind. Aerodyn.*, 51:339–351.

DNV (2022). Maritime forecast to 2050 – energy transition outlook 2022. Technical report, Download at https://www.dnv.com/publications/.

Gerritsma, J. and Beukelman, W. (1979). Analysis of the resistance increase in waves of a fast cargo ship. Technical Report 169S, Netherlands Ship Research Centre.

Gershanik, V. I. (2011). Weather routing optimisation–challenges and rewards. *Journal of Marine Engineering and Technology*, 10(3):29–40.

Gould, R. W. F. (1982). The estimation of wind loads on ship superstructures. *The Royal Institution of Naval Architects*, 8:1–34.

Harvald, S. A. (1983). *Resistance and Propulsion of Ships*. John Wiley & Sons.

Hieminga, G. and Luman, R. (2023). Synthetic fuels could be the answer to shipping net-zero goals, but don't count on them yet. Technical report, Download at https://think.ing.com/.

Hitchcock, D. B. (2003). A history of the metropolis–hastings algorithm. *The American Statistician*, 57(4):254–257.

HSVA (2020). Development of an automated test procedure for efficient determination of roll damping of ships equipped with bilge keels (autoroll). Technical Report 1695, HSVA.

IMO (2023). Resolution mepc.377(80): The 2023 imo strategy for the reduction of greenhouse gas emissions from ships. Download at https://wwwcdn.imo.org/localresources/en/MediaCentre/PressBriefings/Documents/Resolution20MEPC.377(80).pdf.

International Energy Association (2023). World energy outlook 2023. Technical report, Download at https://iea.blob.core.windows.net/assets/ed1e4c42-5726-4269-b801-97b3d32e117c/.

Isherwood, R. M. (1972). Wind resistance of merchant ships. *Trans. of the Royal Institution of Naval Architects*, 38:114–327.

Larsson, A. (2023). Containers lost at sea 2023 update. Technical report, Download at https://www.worldshipping.org/statements/containers-lost-at-sea-2023-update.

Maurício, F. and Moreira, M. (2022). Optimization of sailboat routes under non-uniform wind velocity fields. *Trends in Maritime Technology and Engineering*, pages 391–396.

Metropolis, N., Rosenbluth, A. W., Rosenbluth, M. N., Teller, A. H., and Teller, E. (1953). Equation of state calculations by fast computing machines. *The journal of chemical physics*, 21(6):1087–1092.

Neves, R. J. J. (1985). *Étude experimentale et modélisation des circulations transitoire et résiduelle dans l'estuaire du Sado*. PhD thesis, Univ. Liége.

Press, W. H. (2007). *Numerical recipes 3rd edition: The art of scientific computing*. Cambridge university press.

Ribeiro e Silva, S. and Eça, L. (To be published in 2024). Solution verification of cfd simulations of a drowning body at sea. In *Proceedings of the ASME Symposium on Verification, Validation, and Uncertainty Quantification Symposium (VVUQ 2024)*, Texas, USA.

Ribeiro e Silva, S., Uzunoglu, E., Guedes Soares, C., Marón, A., and Gutierrez, C. (2011). Investigation of the hydrodynamic characteristics of asymmetric cross-sections advancing in regular waves. In *Proceedings of the 30th International Conference on Ocean, Offshore and Arctic Engineering (OMAE 2011)*, Rotterdam (The Netherlands).

Ribeiro e Silva, S. B. N. (2008). *Instabilidades no Comportamento Dinamico Nao-Linear de Navios no Mar*. PhD thesis, Instituto Superior Técnico, Universidade Técnica de Lisboa. In Portuguese.

Salvesen, N. (1978). Added resistance of ships in waves. In *Journal of Hydronautics*, volume 12(1), pages 24–34.

Scheekluth, H. and Bertram, V. (1998). *Ship Design for Efficiency and Economy*. Butterworth & Heinmann.

APPENDIX

The vessel studied in here corresponds to a 712 TEU geared containership, whose $Fn = 0.26$. As regards the case-study selection, containerships are the highest emissions producers in the world fleet due to their higher sailing speed that requires larger propulsion engines.
Considering the design load condition of 712 TEU, the main characteristics of the vessel are shown in Table 2.

Table 2: Main characteristics of the 712 TEU geared containership.

Length between perpendiculars	L_{pp}, in [m]	119.50
Breadth, maximum	B, in [m]	20.4
Draught, mean	T_m, in [m]	7.75
Displacement, light condition	Δ_l, in [t]	3936
Crew	N_{crew}, in [pax]	16
Gross tonnage	GT, in [t]	7580
Cargo capacity	N_{TEU}, in [TEU]	712
Crane elevation capacity (x2)	C_{crane}, in [t]	40
Power (effective)	P_E, in [kW]	4665
Power at MCR (shaft)	P_S, in [kW]	7200
Propeller diameter (CPP)	D_P, in [m]	4.2
Cruise speed	U_{cruise}, in [kts]	16
Lateral projected area (above MWL)	A_L, in [m^2]	1883
Transverse projected area (above MWL)	A_T, in [m^2]	444

Fig. 13 shows a 3D geometric model which has been utilised to perform the CFD resistance and propulsion simulations and the semi-empirical wind loads calculations of the vessel. Considering the origin of the right handed system of coordinates located along the ship keel, in the symmetrical plan, at mean distance between the two perpendiculars, with z-axis pointing upwards and x-axis pointing through the ship bow.

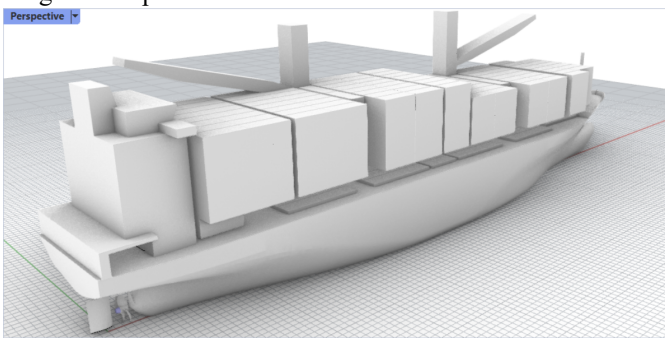

Figure 13: 3D geometric model of the containership.